



Seismic and aseismic slip during the 2006 Copiapó swarm in North-Central Chile



Javier Ojeda ^{a,b,c,*}, Catalina Morales-Yáñez ^d, Gabriel Ducret ^e, Sergio Ruiz ^b, Raphael Grandin ^a, Marie-Pierre Doin ^f, Christophe Vigny ^g, Jean-Mathieu Nocquet ^{h,a}

^a Université Paris Cité, Institut de Physique du Globe de Paris, CNRS, Paris, France

^b Departamento de Geofísica, Universidad de Chile, Santiago, Chile

^c Departamento de Geología, Universidad de Chile, Santiago, Chile

^d Departamento de Ingeniería Civil, Universidad Católica de la Santísima Concepción, Concepción, Chile

^e Institut Français du Pétrole Energies Nouvelles, Rueil-Malmaison, France

^f Université Grenoble Alpes, Université Savoie Mont Blanc, CNRS, IRD, Université Gustave-Eiffel, IsTerre, Grenoble, France

^g Laboratoire de Géologie - CNRS UMR 8538, École Normale Supérieure - PSL University, Paris, France

^h Université Côte d'Azur, Géoazur, IRD, CNRS, Observatoire de la Côte d'Azur, Valbonne, France

ARTICLE INFO

Keywords:

Seismic swarm

Short term slow slip event

Aseismic deformation

Subduction zone processes

Copiapó

Chile

ABSTRACT

Earthquake swarms commonly occur along the Chilean subduction zone, witnessing fast seismic and slow aseismic slip behavior at the plate interface. However, the largest seismic swarms observed in Chile, particularly in the Copiapó-Atacama region, remain poorly documented, and the underlying processes have yet to be understood. Here, we perform seismological and geodetic analyses to investigate the 2006 Copiapó swarm, which developed in April and May 2006. The swarm began on April 19, with a magnitude M1 5.3 earthquake. During the nine following days, we observe a migration of seismicity along the plate interface, the occurrence of doublets events, and a potential slow slip event in the GPS time series at site Copiapó. Then, on April 30, a first earthquake with Mw 6.6 occurred at 15 km depth at the plate contact. It likely triggered a second earthquake of magnitude Mw 6.5, which occurred 144 min later, 10 km northwest of the first earthquake. Using InSAR, we determined the slip distribution associated with these two earthquakes and detailed the postseismic slip they triggered in the next days and weeks. This “postseismic” phase appears to be predominantly aseismic, while the moment released during the “coseismic” phase is comparable to other seismic crises that occurred in Atacama. Although we did not find a larger seismic and aseismic ratio than in other swarms in South America, we suggest a similar mechanism of slow deformation as a driver of seismicity during seismic swarms. Finally, we propose that the slow and fast behavior of the 2006 Copiapó swarm is a consequence of the subduction of the Copiapó Ridge seamounts, which affects both the plate interface and the overriding plate by inducing complex interactions between seismic and aseismic processes.

1. Introduction

The North-Central Chile subduction zone is characterized by significant background seismicity, the occurrence of large earthquakes, and episodic seismic swarms that reflect the wide variability of slip behavior in this tectonic setting. Previous studies propose that the bathymetric heterogeneities along the subducting plate, such as fracture zones or oceanic ridges, could explain the diversity of the slip modes and also the along strike segmentation in subduction zones (e.g., Poli et al., 2017; Maksymowicz, 2015; Pastén-Araya et al., 2022). Indeed, oceanic

features such as fracture zones have been related to the presence of hydrated sediments and fluids (e.g. Peacock, 1990; Manea et al., 2014; Nishikawa and Ide, 2015). Seamounts and oceanic ridges impact the dynamics of subduction zones (Morell, 2016) defining potential barriers to large seismic ruptures (e.g. Contreras-Reyes and Carrizo, 2011; Das and Watts, 2009). These interpretations led to correlate the presence of these subducted oceanic features with high pore pressure content inside a fluid-rich system that may drive the observed diversity

* Corresponding author at: Université Paris Cité, Institut de Physique du Globe de Paris, CNRS, Paris, France.

E-mail addresses: ojeda@ipgp.fr (J. Ojeda), catalina.morales@ucsc.cl (C. Morales-Yáñez), gabriel.ducret@ifpen.fr (G. Ducret), sruiz@uchile.cl (S. Ruiz), grandin@ipgp.fr (R. Grandin), marie-pierre.doin@univ-grenoble-alpes.fr (M.-P. Doin), vigny@biotite.ens.fr (C. Vigny), nocquet@geoazur.unice.fr (J.-M. Nocquet).

of slip modes and, more especially, those related to seismic swarm activity (Nishikawa and Ide, 2017).

The Copiapó-Atacama area hosted large earthquakes (Fig. 1). Archaeological and paleoseismological inferences from Salazar et al. (2022) allowed them to identify a mega-earthquake that occurred ~3800 yrs ago, which may explain the awareness and lifestyle changes of the inhabitants along the coastal area of northern Chile. Besides, the 1420 Oei orphan tsunami could possibly be attributed to a great earthquake magnitude M8.8–9.4 (Abad et al., 2020) along the Atacama segment. Other large earthquakes occurred in 1819 (Ms 8.3) and 1922 (Mw 8.5–8.6) (Beck et al., 1998; Kanamori et al., 2019; Carvajal et al., 2017), while several earthquakes magnitude M~7 or similar have been reported in 1796, 1859, 1909, 1918, 1946, and 1983 (Comte et al., 2002; Ruiz and Madariaga, 2018). Recent studies have shown that the Atacama segment experiences both seismic and aseismic slips. Klein et al. (2018a) detected a slow slip event (SSE) between 2014 and 2016 below the city of Copiapó, representing the first deep long-term SSE documented in Chile. The deep SSE is located in a low coupled zone (Klein et al., 2018b; Métois et al., 2014), and exhibits a potential recurrent pattern of about 4–5 years since the same transient signal was recorded by a continuous GPS station in 2005, 2009, 2014 and more recently in 2020 (Klein et al., 2023). Interestingly, seismic and aseismic signatures have also been observed through the seismicity distribution, non-volcanic tremors, and repeaters events. Those signals are placed in areas of Vp, Vs, and Vp/Vs ratio anomalies, pointing out the subduction of the Copiapó Ridge as an important bathymetric feature controlling the along-strike and along-dip changes of slip behaviors (Pastén-Araya et al., 2022). The Copiapó Ridge, built by hotspot tracks in the Nazca plate, is characterized by a rough and discontinuous topography that formed its seamounts. This oceanic feature had different migration episodes in the last 60 Ma that coincides with the southward migration of the flat slab, suggesting a key role of oceanic ridges such as Copiapó, Juan Fernández, or Tal Tal in the deformation process along North-Central Chile (Bello-González et al., 2018).

Over the last 50 years, repeated occurrences of seismic sequences and seismic swarms have been observed in the Atacama region (see Fig. S1). For instance, the sequences occurring at latitudes 27.5°S – 28°S in 2002, 2011, and more recently during 2020 in Vallenar-Atacama (Klein et al., 2021) or the swarm episodes of 1973, 1979, 2006 (Comte et al., 2002; Holtkamp et al., 2011), and 2015 offshore the cities of Caldera and Copiapó at latitudes 26.7°S – 27.5°S (Fig. 1, see Fig. S1). Precisely in Copiapó, one of the most productive seismic swarms that have been observed in Chile and South America occurred between April and May 2006. The Copiapó area is characterized by low Vp and high Vp/Vs (Comte et al., 2006), indicating the presence of fluid-richness, spatially correlated with the location of a subducting seamount. Furthermore, Holtkamp et al. (2011) used the NEIC seismic catalog and InSAR imagery to analyze the 2006 seismic swarm, estimating a seismicity migration of about ~7 km/day during the sequence, but also suggesting that the observed ground deformation could not require an important contribution of aseismic slip. However, it remains unclear how the Copiapó swarm evolved spatiotemporally and whether the scarce seismological local data and geodetic observations can reveal any component of aseismic slip.

In this study, we revisit the fast and slow processes during the 2006 swarm (Fig. 2) that occurred offshore the cities of Copiapó and Caldera in the Atacama region, North-Central Chile. The seismic swarm initiated on April 19, with an earthquake magnitude Ml 5.3 accompanied by doublet earthquakes and a slight westward transient in the single GPS station available in the area. After a few days of lower intensity in the seismic activity, the two largest earthquakes magnitude Mw~6.5–6.6 occurred on April 30, separated by 2.4 h. We used the available geodetic and seismological data to understand the slip behavior that drove this swarm. Our analysis shows that the Copiapó swarm produced complex interactions along the plate interface, which may be accompanied by a possible short-term SSE. The swarm is spatially correlated with a subducted oceanic seamount, possibly responsible for the seismicity pattern through time.

2. Data and methods

2.1. Regional seismic data and processing

To perform our seismological analysis, we used regional short-period, three-component seismic stations deployed by the National Seismological Service of the Universidad de Chile (SSN: Servicio Sismológico Nacional), now the National Seismological Center (CSN: Centro Sismológico Nacional, Barrientos, 2018). Using this network, the SSN performed hypocentral location and magnitude estimation of the seismic swarm, including some earthquakes Ml~2–3 well recorded by near-field seismic stations (Fig. 2a and Fig. S2). The raw waveforms used for picking and locating the earthquakes were archived by the SSN, including trimmed waveforms for 32 seismic stations and P-wave or S-wave pick arrivals. In this study, we consider the CSN catalog due to the spatial station distribution and large gap window to characterize the offshore swarm activity. This drawback does not allow us to improve the hypocentral locations using algorithms such as the double-difference method. Unfortunately, there are no continuous records from these seismic stations to search for microseismicity, except two broadband GSN (Global Seismological Network) stations: LCO (Las Campanas) and LVC (Limón Verde), located 200 and 550 km-distance from the seismic swarm source, respectively (see Fig. S2). Although both stations have good quality data, the long source-station distance and the significant data gaps during the study period made it difficult to observe any small signal associated with the seismic swarm.

We aimed to assess for possible slip accelerations during the seismic swarm by analyzing the possible occurrence of repetitive seismicity surrounding asperity areas. For this, we further attempted to study the presence of repeater and/or near-repeating earthquakes in our catalog by performing cross-correlations between pairs of events. We considered 180 pairs of events recorded by the three components of the nearest stations CDCH, CRCH, and CPCH (Fig. 2a). Afterward, we followed a standard pre-processing scheme involving detrending, tapering, bandpass filtering between 2 and 8 Hz, and resampling of the seismic signals. The chosen frequency band includes the corner frequency of the entire seismicity of our dataset, which allowed us to characterize the repeater and/or near-repeating earthquakes (Uchida, 2019; Uchida and Bürgmann, 2019) (see Fig. S4). We considered a time-window from 1 s before the P arrival to 9 s after the S arrival of the normalized processed waveforms and correlate the pairs of events. Finally, we took the maximum cross-correlation for the station and the arithmetic average among them.

2.2. W-phase moment tensor inversion

We computed the moment tensor and the centroid location of the two most significant earthquakes of the seismic sequence, which occurred on April 30 at 19:17 and April 30 at 21:41 (hereafter first and second event). Thereby, we performed a source inversion using the W-phase inversion algorithm (Duputel and Rivera, 2019). The algorithm focuses on finding the solution with the minimum root mean square (RMS) of the waveform misfits. We used teleseismic waveforms from stations with an epicentral distance from 0° to 90° of the worldwide network Incorporated Research Institutions for Seismology (IRIS, available at <http://ds.iris.edu/wilber3>, Fig. 2b). The time window used is the standard for W-phase inversion, which begins with the P-wave arrival, and has a duration of $\delta t = 15 \times \Delta$, where Δ corresponds to the epicentral distance. We filtered the data with a causal bandpass Butterworth filter of order 4. The frequency band used corresponds to 100–250 s and 100–200 s for the first and second events, respectively. We chose these frequency bands following the work of Duputel and Rivera (2019) and considering the signal-to-noise ratio of each event.

To obtain the focal mechanism, we first performed an initial inversion using the solution given by the Global Centroid Moment Tensor (GCMT, Ekström et al., 2012; Dziewonski et al., 1981) catalog as

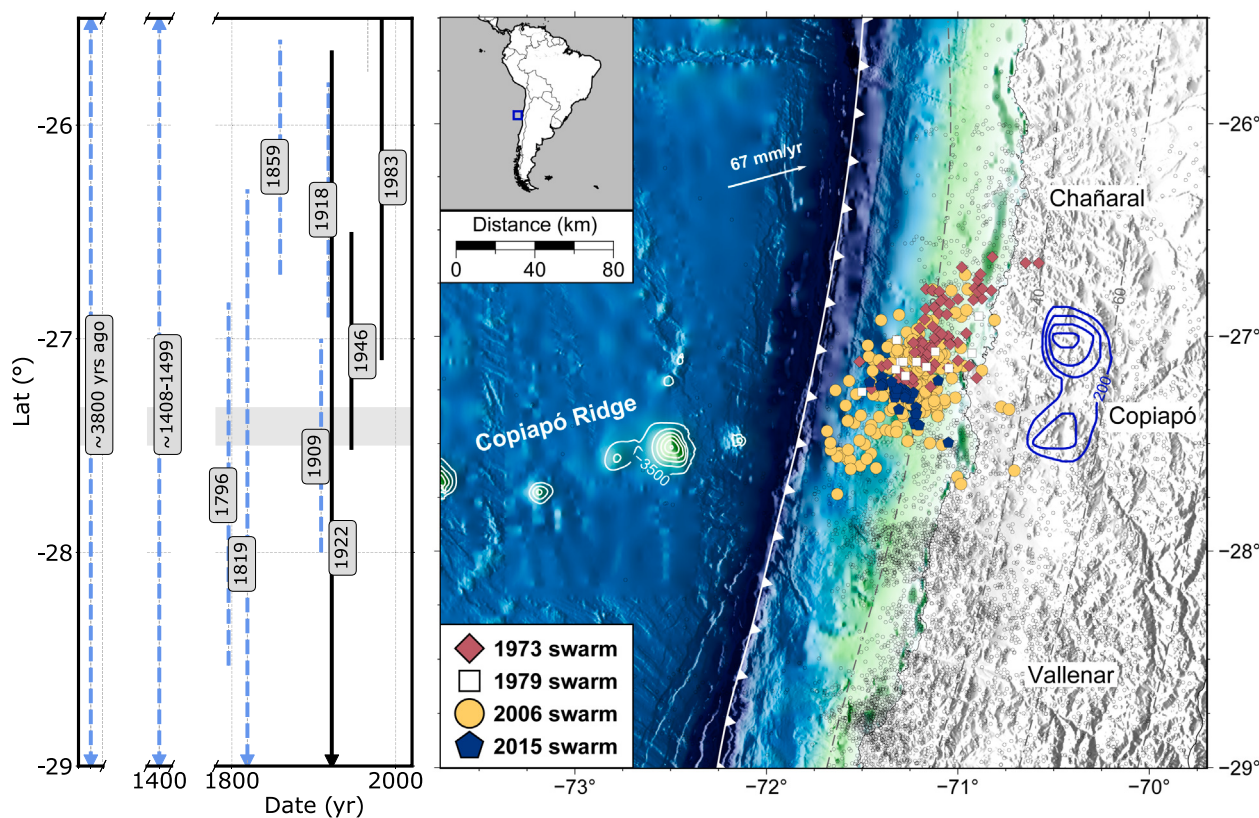


Fig. 1. Overview of the study area; see the inset map showing the location with reference to South America. The segmented blue lines in the left panel indicate the rupture length of pre-historic, historical, and recent earthquakes (Comte et al., 2002; Ruiz and Madariaga, 2018; Abad et al., 2020; Salazar et al., 2022). The right panel indicates the seismotectonic context in the Copiapó region. The red, white, yellow, and blue symbols indicate the seismicity location of the 1973, 1979, 2006, and 2015 seismic swarms, respectively. The gray dots indicate the seismicity that occurred between 1900 and 2022, database compiled by USGS and CSN. The blue lines are the 50 mm iso-contour slip of the 2014 deep SSE (Klein et al., 2018a). The white lines on the bathymetry indicate the 500 m iso-contour depth of the heterogeneous seamounts associated with the Copiapó Ridge. The white triangles indicate the trench, and the segmented black lines represent the Slab2 model of the South America subduction zone (Hayes et al., 2018).

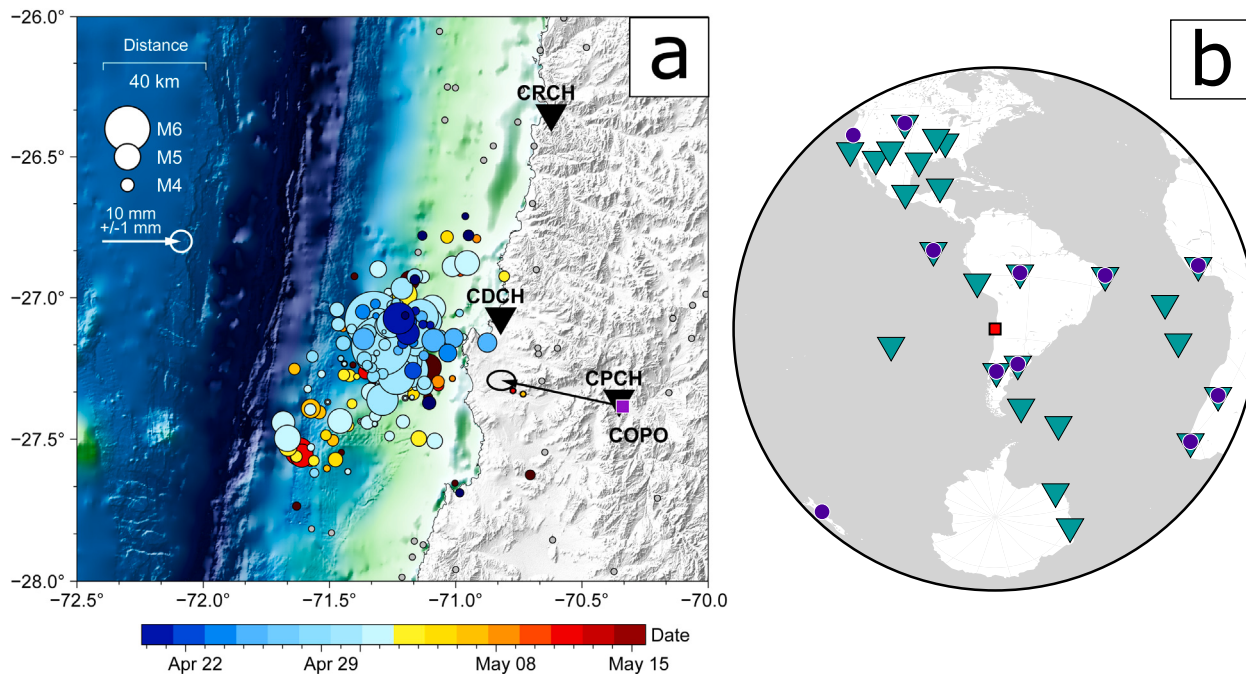


Fig. 2. Available datasets during the 2006 Copiapó swarm. (a) The black inverse triangles are the regional short-period, three-component seismic stations; the purple square is the GPS station installed in Copiapó. The arrow and ellipse indicate the horizontal displacement due to the Mw~6.5–6.6 earthquakes on April 30 and the respective horizontal error (Klein et al., 2022). The circles represent the seismicity between 2006-04-19 and 2006-05-15, colored by the date of occurrence during the seismic swarm and sized by the magnitude of each event; gray dots are seismicity not related to the swarm. (b) Distribution of teleseismic stations used in the W-phase inversion for the two largest events of the seismic swarm: bright cyan inverted triangles for the 2006-04-30 19:17 event and purple circle for the 2006-04-30 21:40 event.

preliminary information. We performed automatic and manual waveform selection to exclude noisy or incomplete data. After data screening, solutions were obtained using 30 and 14 channels for the first and second event, respectively. We then performed a second solution and iterated in space and time to determine the centroid position and W-phase moment magnitude (M_{WW}). Once we have the best hypocentral location, we run the algorithm to compute the focal mechanism at different depths to analyze the solutions.

2.3. GPS data

At the time of the 2006 seismic swarm, station COPO, located at a ~ 100 km distance eastward from the seismic swarm source, was the only single available continuous GPS site operating in the Copiapó area (Fig. 2a). This site was installed on 2002-07-01 and shut down on 2015-08-05 (Fig. S5). Although the COPO station has large gaps in its records between 2007-10-01 and 2008-07-03, we detected a few days of data gaps during the 2006 seismic swarm: 2 days before and after the two largest earthquakes of the sequence.

We used the GPS time series from the database SOAM_GNSS_soleNS (Klein et al., 2022), which provides time series of precise daily station positions obtained from double-difference processing expressed with respect to ITRF14. This dataset has been used recently to develop precise time-dependent afterslip evolution after large earthquakes (Tissandier et al., 2023), as well as to identify transient signals along the northern Chile subduction zone (Klein et al., 2023). Here, we used a time-window from February to July 2006 for the horizontal components of the COPO station; afterward, we detrended the COPO time series using the velocity estimated from 2 months before April 19, the date we identified as the beginning of the seismic swarm.

2.4. InSAR data and modeling

Synthetic Aperture Radar (SAR) data were acquired by the European Space Agency's ENVISAT satellite track 96. Due to the sparse temporal coverage of the area, and the small magnitude of the deformation, a specific strategy has to be used to separate tectonic signals from non-tectonic perturbations (tropospheric delays, ionospheric delays, and orbital ramps). We computed interferograms with a small baseline strategy, requiring a closure of the interferometric network while adapting the different steps to the irregular latitudinal coverage of the dataset (Fig. S6a). We first coregistered all images with respect to a single primary image, using intermediate primary images to connect the most distant acquisitions (in space and time, Fig. S6b). This constraint led us to include a total of 55 interferograms with perpendicular baselines reaching up to 585 m and temporal baselines up to 5 years. To maintain an acceptable level of coherence and facilitate phase unwrapping, we corrected the interferograms from DEM errors (Ducret et al., 2013) and subtracted stratified atmospheric delays derived from ERA-Interim (Jolivet et al., 2011). After applying a moving-average filter, we ran an iterative unwrapping procedure guided by coherence, as described in Grandin et al. (2012).

Finally, after unwrapping, we estimated parameters of phase ramps in azimuth and in range, and inverted for those parameters in a network fashion to ensure a consistent correction of all interferograms. Prior to parameter estimation, interferograms were clipped to discard phase values evidently affected by a local atmospheric artifact, and measurements in the area of the Copiapó swarm were masked to avoid contaminating the phase ramp estimation with a potential tectonic signal. For the azimuth ramp, we used a cubic fit as a function of azimuth coordinate for "long" interferograms (i.e. exceeding ~ 400 km along-track), whereas a quadratic fit was used for "short" interferograms. Because the images are narrower in the range dimension, the orbital ramps in the range were modeled as linear.

After interferogram correction, the majority of atmospheric and orbital artifacts were expected to be mitigated. However, the topography of the area is characterized by an east–west elevation gradient that translates, in the presence of a strong stratified component of atmospheric delays, into a steep phase ramp in range. Hence, uncertainty on the atmospheric corrections mapped into a bias in the empirical ramp corrections. In order to further improve the orbital and atmospheric corrections, we performed a time-series inversion of the interferogram network, incorporating (1) a smoothness constraint in time, (2) a linear phase-elevation term with a coefficient varying linearly with azimuth (to account for the latitudinal change in atmospheric phase screen), and (3) a linear ramp in range with a coefficient varying linearly with azimuth (which yields a skewed phase ramp).

3. Results

3.1. Migration of seismicity

The quality of the manual picks was good enough to identify the main characteristics of the seismic swarm. Using the trimmed raw waveforms for 32 seismic stations (see Fig. S2), we were able to identify 2470 pick arrivals, either P or S phases performed by the SSN, between February 28 and June 1 in the study area (Fig. 2), with a total of 312 events. We then used the hypocentral location of the seismicity, discriminating those earthquakes associated with the seismic swarm both in space and time. Fig. 3 shows the spatiotemporal evolution of the seismicity between April and May 2006 associated with the Copiapó swarm; in this figure, the main reference is the event that occurred on April 19, M_L 5.3, which we identified as the first event of the whole seismic swarm. After this event, all subsequent seismicity during the next nine days occurred within a localized zone along latitude and longitude (Fig. 3b, and 3c, respectively). The view of a clustered seismicity is also supported by the observed similarity in S-P time during the same period at the coastal stations CDCH and CRCH; nonetheless, at inland station CPCH, these results are not clear due to the long distance from the seismic swarm source (Fig. S3). Although the final catalog includes 235 events with magnitudes between M1.7–6.6, the magnitude of completeness is about M3.7.

We calculated the radial distance from the epicentral position of the event that occurred on April 19 (Fig. 3d). During this day, we observed a clustered seismicity propagated at fast velocities in both directions, eastward and westward the first shock. However, following the next ten days after this cluster (Fig. 3d), we identified mainly two patterns: (1) an eastward migration (greenish circles) at velocities between 2 to 10 km/day and (2) a westward migration (pinkish circles) at velocities about 2 to 5 km/day. Interestingly, during the same period between April 19 to April 28, we observed a slightly westward motion of about 2 mm in the time series of the GPS station COPO (Fig. 4). There were no changes in the north-south component.

We further investigated possible additional signatures of slow deformation to support the slightly westward trend of the COPO station. First, we studied the possible presence of repeating earthquakes, similar events, or doublets in our database. We found doublet events in the frequency band between 2–8 Hz using the three closest stations to the seismic swarm source. We obtained only four pairs of events with correlation coefficients greater than or equal to 0.85 (Fig. 5 and Fig. S7). The highly correlated doublet ($cc = 0.97$) occurred on April 19, when we identified the beginning of the seismic swarm, with two events magnitudes M_L 2.9 and M_L 3.3 (Fig. 5b). After considering all possible pairs of events recorded by the three-component three stations CDCH, CPCH, and CRCH (in total, there are 180 earthquakes during the period analyzed), we built a similarity matrix that contains the correlation coefficient for all the event numbers (Fig. 5a). Here, we noticed that during the first days of the seismic swarm, between April 19 and April 20, the correlation coefficient was the highest of all the periods, including values larger than 0.5, suggesting highly clustered

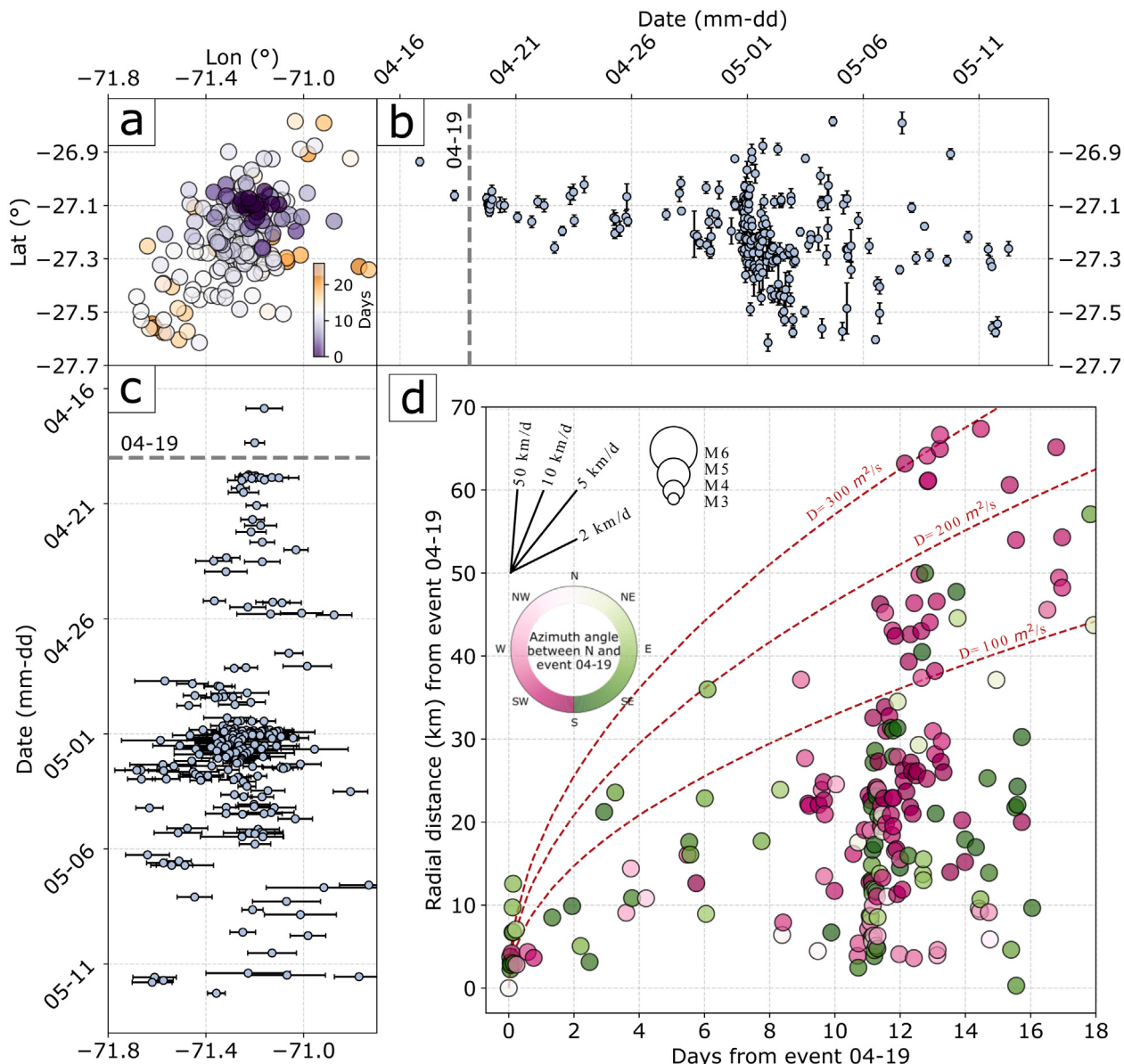


Fig. 3. Spatiotemporal analysis of the 2006 Copiapó swarm. (a) Aerial view of the seismicity colored by date and sized by magnitude. The seismicity evolution from mid-April to June is indicated by (b) latitude in blue circles and (c) longitude in red circles; error bars are indicated for each event. (d) Radial spatial migration (measured from the event 2006-04-19) as a function of days. The black lines indicate migration velocities of 2, 5, 10, and 50 km/day. Red dashed lines are the fluid diffusion curves from Shapiro et al. (1997) using a hydraulic diffusivity (D) of 100, 200, and 300 m^2/s , representing the 98-, 95-, and 82-percentile of the seismicity, respectively. The white circle indicates the magnitude of the earthquakes from M3 to M6. The color of each circle is related to the azimuth angle between the N and the position of the 2006-04-19 event, as shown in the polar colorbar.

activity. Overall, we retrieved doublets events and seismicity increase that could indicate the presence of slow slip in the area. Although we expected the presence of repeater earthquakes through time, the high magnitude threshold and the lack of continuous records reduce our detection capability of such signals.

On April 28 (day 9), a new series of earthquakes started, migrating southwest (pinkish circles on Fig. 3d) while the clustered seismicity started spreading in latitude and longitude. Then, the spreading of the seismicity was mainly affected by the two largest earthquakes of the whole sequence that occurred on April 30 at 19:17 UTC and 21:40 UTC. The earthquakes produced an offset of about 15 mm at the east–west component and 3 mm at the north–south component of the COPO GPS station. We analyzed these earthquakes in Section 3.2. On May 2 (day 13, Fig. 3d), seismicity continues growing to the southwest, forming a secondary cluster near 71.6°W, 27.4°S (Fig. 3a). However, during this period, we cannot observe any noteworthy trend in the COPO time

series other than the postseismic afterslip promoted by the two largest events mentioned above, mainly observed in the east–west component (Fig. 4).

3.2. The two largest earthquakes within the swarm

We studied the two largest events of the sequence. Both events magnitude $M_w \sim 6.5$ –6.6 occurred on April 30, only 2.4 h apart. Other seismological agencies, such as GCMT or NEIC, show substantial differences in the magnitude, depth, and location of these earthquakes. The regional records at stations CDCH, CPCH, and CRCH (see Fig. S8) show only minor amplitude, shape, and time signal differences. However, the regional data were insufficient to perform this analysis; we employed a W-phase inversion using teleseismic records to characterize the seismic source of these events.

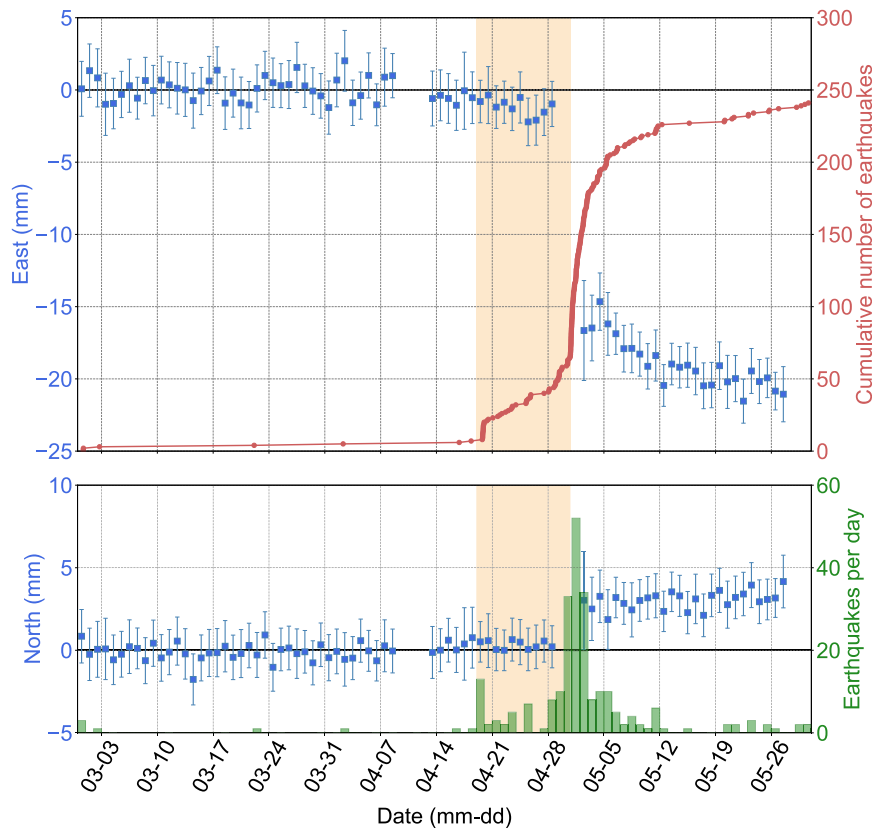


Fig. 4. GPS displacement at station COPO for the east-west and north-south components (blue squares of top and bottom panels, respectively), error bars are indicated for each daily solution. The red curve (top panel) and green curve (bottom panel) correspond to the cumulative number of earthquakes and earthquakes per day, respectively. The orange area shows the period 2006-04-19 and 2006-04-30, before the largest earthquakes of the seismic sequence.

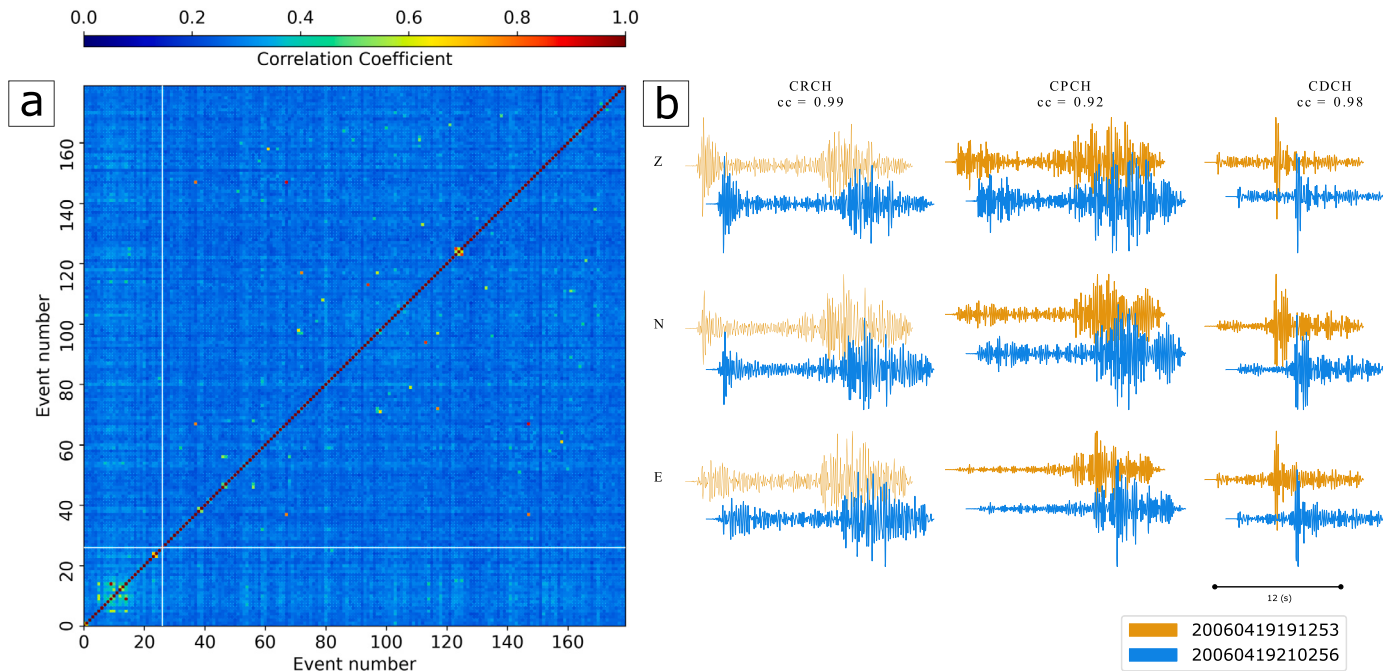


Fig. 5. Analysis of doublets within the seismic swarm. (a) Similarity matrix for 180 pairs of events recorded by the three closest stations CDCH, CPCH, and CRCH. The Event number is sorted by the origin time of events. Event 0 and Event 180 correspond to the 2006-02-28 and 2006-06-01 events, respectively. The vertical and horizontal white lines indicate the event 2006-04-22 16:03:29. (b) Example of doublet for the Copiapó swarm, with a correlation coefficient larger than 0.97 considering three-components waveform cross-correlation (pair 2006-04-19 19:12:53, 2006-04-19 21:02:56).

The inversion solution localizes the centroid of the first event at 27.17°S, 71.3°W and the second event at 27.08°S, 71.33°W (Fig. S9a,

c). The iteration in time shows that the time shift corresponds to 6.0 s and 7.0 s for the first and second events, respectively (Fig. S9b,

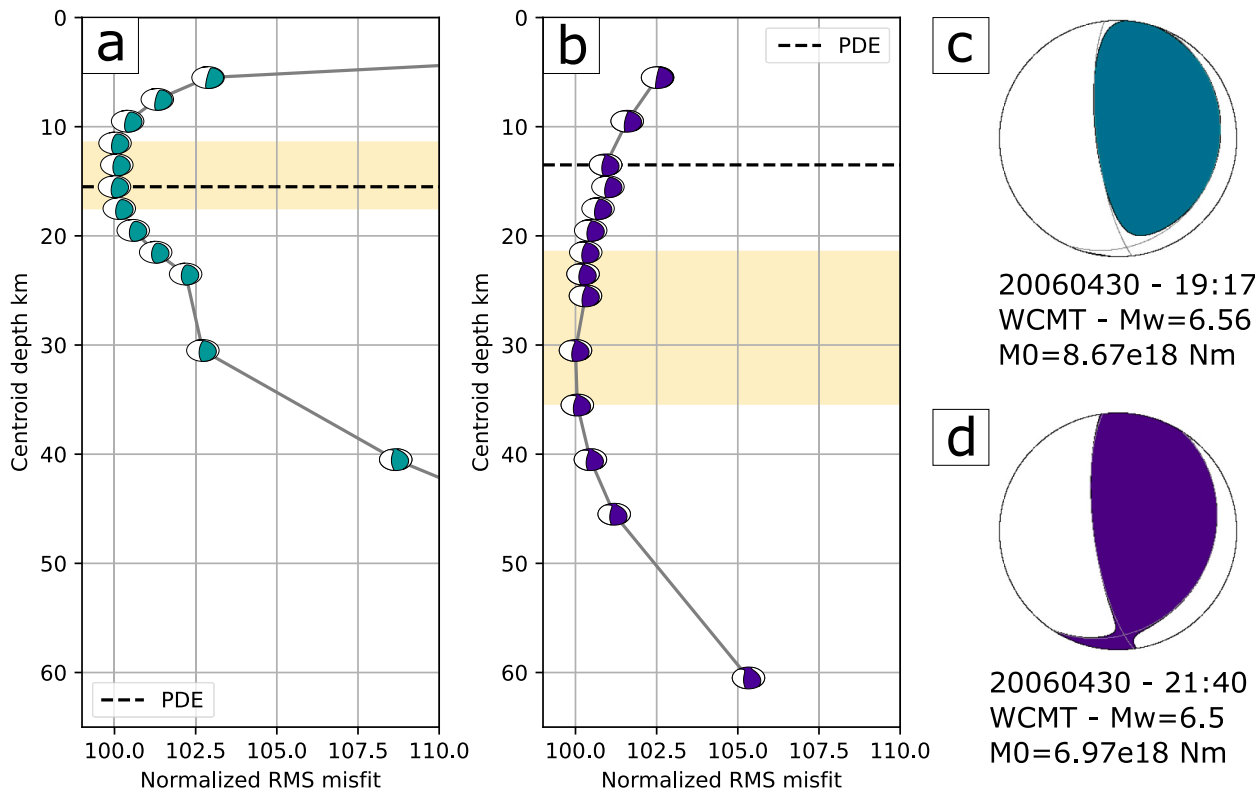


Fig. 6. W-phase inversion for the 2006-04-30 19:17 (bright cyan color) and 2006-04-30 21:40 (purple color) earthquakes. Centroid depth grid search for (a) the first event and (b) the second event. The black and blue lines represent the preliminary determination of epicenter (PDE) from GCMT and optimal solutions obtained from the WCMT inversions. Preferred solutions for (c) the first earthquake and (d) the second earthquake.

d). The waveform fit of each solution is shown in the supplementary material in Fig. S10 (for the first event) and Fig. S11 (for the second event). Furthermore, Fig. 6 summarizes the W-phase inversion of the first and second events. The figure shows the focal mechanism of the earthquakes at different depths as a function of the normalized root mean square misfit ($\frac{rms}{min(rms)} \times 100$) and the best solution in each case. Around the best-fit solutions, the obtained moment tensor is similar. Moreover, the first event depth between 11–17 km presents the lowest misfit values (Fig. 6a), while for the second event, the lower misfit appears in the range between 23–35 km depth (Fig. 6b). The differences in the depth range might be due to the low signal-to-noise ratio, in addition to the poor quality seismograms recorded for the second event, which are mixed with the surface waves of the first event. Fig. 6c, d also shows that the rupture mechanism of both events corresponds to a reverse fault with a magnitude Mww 6.56 and Mww 6.5, respectively.

3.3. Coseismic and postseismic deformation from InSAR and GNSS data

The result of the time-series inversion, after removing the atmospheric and orbital components, is displayed in Fig. S12, plotted using reference images before (Fig. S12a) and after (Fig. S12b) the 2006 Copiapó swarm. The difference in deformation that occurred between the two consecutive acquisitions, bracketing the time of the Copiapó swarm, is evident (2005-09-26 and 2006-07-03). However, the long temporal window between these images hinders a detailed quantification of this deformation event.

We also observed that deformation continued during the two time periods that followed the main time-step of it (between 2006-07-03 and 2006-08-07, and between 2006-08-07 and 2007-03-05). This observation is consistent with the abnormal motion detected at GPS station COPO in the ~6 months following the swarm (Figs. 2 and 4). In order to further separate this instantaneous deformation from an additional transient signal, we applied a parametric pixel-wise inversion of the

cumulative deformation time series (after discarding non-tectonic signals). We assumed that the time-series consists in the superposition of (1) a Heaviside function at the time of the earthquake (the “coseismic” component), (2) a linear transient taking place in a time-interval of finite duration after the earthquake (the “postseismic” component) and (3) a constant (the “reference image” phase screen). We did not incorporate an interseismic trend in the inversion to avoid a trade-off with the postseismic component, whereas accounting for a more realistic temporal evolution of the postseismic transient (logarithmic, exponential) leads to similar results for the total displacement of the transient.

The result of this signal separation procedure is shown in Fig. S13. The coseismic component is characterized by increasing displacement (away from the satellite) towards the area affected by the Copiapó swarm, reaching a maximum of approximately 5 cm in the LOS at the coast. The postseismic component has a similar spatial distribution, albeit peaking inland, with a smaller displacement (maximum 3 cm). This result is consistent with the analysis of Holtkamp et al. (2011), although our exhaustive exploitation of the whole ENVISAT dataset allows for a better separation of signals. Based on their spatial pattern, both the co- and postseismic patterns are consistent with slip on the subduction interface taking place offshore or under the coast at the latitude of the Copiapó swarm.

In order to quantify the spatial distribution of slip associated with the co- and post-seismic components, we invert for slip on the subduction interface, incorporating both the InSAR-derived displacements and the displacement estimated from GPS station COPO. For the latter estimation, we extract the horizontal vectors in the two time intervals defined from the InSAR temporal coverage by fitting the same temporal functions (interseismic trend, coseismic step, postseismic transient) on the COPO time series. We obtain a “coseismic” displacement of −1.6 cm EW and 0.4 cm NS, and a “postseismic” displacement of −0.7 cm EW and −0.2 cm NS (with 1-sigma uncertainties of 0.2 cm).

The inversion uses the equations of Okada (1985), following the same approach presented by Ruiz et al. (2013). However, the small signal-to-noise ratio of the InSAR and GNSS datasets requires to incorporate constraints in the inversion to mitigate instabilities. We choose to apply a total seismic moment constraint, whereby the integrated slip on the interface has to match a prescribed geodetic moment (which can be converted to a seismic moment by multiplying by an appropriate value of the shear modulus). For the “coseismic” inversion, we force the slip distribution to match a seismic moment of $2.3 \cdot 10^{19}$ Nm (assuming a shear modulus of 30 GPa), which corresponds to the cumulative seismic moment released during the “coseismic” phase (representing an equivalent magnitude Mw 6.8). For the “postseismic” inversion (after 2006-07-03), the cumulative seismic moment released by local earthquakes (equivalent to Mw 5.4) is insufficient to match the quantity of deformation measured at the surface, unless slip is occurring at a depth substantially shallower than the plate interface. As a consequence, to comply with the assumption that slip is taking place on the interface, we enhance the seismic moment constraint so as to match an equivalent magnitude Mw 6.5.

The resulting slip distributions, as well as synthetic displacement maps, are shown in Fig. 7. Slip during the “coseismic” phase reaches 40 cm and is constrained between the coast and halfway to the trench. On the other hand, “postseismic” slip occurs on a narrow band aligned along the coast. However, the precise slip distribution remains poorly resolved, especially in its up-dip segment of the subduction interface.

4. Discussion

4.1. Seismic swarm migration and the two largest earthquakes

We analyzed the spatial and temporal evolution of the Copiapó swarm from the day of the first earthquake, the M1 5.3 occurred on April 19, until April 30. In the early stage, the sequence exhibits localized and persistent seismicity in the central area of the whole seismic swarm (Fig. 3a). The epicentral location of these earthquakes is well resolved due to the small latitude and longitude errors (see Fig. S14). The intense clustered seismicity can be interpreted as a burst of seismicity during the first day with a fast migration, likely following an earthquake cascade interaction among small events. After that phase, during the next ten days, the seismicity follows mainly two trends; one toward the east of the location of the first event (greenish circles on Fig. 3d), characterized by high seismicity that migrates at velocities between 2–10 km/day; a second trend toward the trench (pinkish circles on Fig. 3d) that seems to migrate at lower velocities around 2–5 km/day. On the other hand, we further studied the possibility of seismicity migration rates induced by a fluid diffusion migration (Shapiro et al., 1997). Fig. 3d shows the fluid diffusion curves considering hydraulic diffusivity of 100, 200, and 300 m²/s to explain the data. Similar curves have been obtained by Shapiro et al. (2003), who proposed these values as an upper limit for the diffusivity coefficient. In addition, the fluid diffusion processes are expected to be slower than 0.5 km/day, while slow slip fronts show velocities of about a few 3–10 km/day (Hoskins et al., 2021). Thus, these migration velocities are compatible with a slow slip event propagation in subduction zones (e.g., Shelly et al., 2007; Kato et al., 2016).

The migration pattern described above continued until April 30 (day 11), when the two largest earthquakes of the sequence ruptured to the west of the April 19 event. First, at 19:17 (UTC), the earthquake magnitude Mw 6.6 ruptured at shallow depths of around 15 km with an epicentral location at mid-distance between the trench and the coastline. According to the slab 2.0 model, the earthquake occurred at the plate interface. Seismicity followed this earthquake until 144 min after when the second event of magnitude Mw 6.5 ruptured only ~10 km to the northwest from the first event. Due to the closeness of these largest earthquakes, and also considering their rupture size, they could have interacted between them by a triggering process led by the

redistribution of stress. After these events (exceeding the magnitude of the whole swarm), the seismicity exhibits a more organized pattern with an acceleration in the cumulative number of events. Moreover, the persistent and localized seismicity that occurred during the initial period vanished. We instead observe that the seismicity spreads along an apparent north-east to south-west alignment (Fig. 3), which may be connected to the track of the subducted Copiapó ridge and its deformation fingerprint along the plate interface and the overriding plate (Álvarez et al., 2015). Finally, during the last period until mid-May, the seismicity is likely driven by the afterslip triggered by the two April 30 Mw~6.5–6.6 earthquakes.

One question that needs to be addressed is whether the 2006 Copiapó crisis follows the characteristics of a seismic swarm or rather shows a pattern of mainshock–aftershock. Despite our previous observations on the spatiotemporal seismicity evolution, we agree with Holtkamp et al. (2011) that the 2006 Copiapó crisis as a whole could be described as a seismic swarm; firstly, the largest earthquakes in the sequence occurred in the middle of the sequence; secondly, the total area of the seismic swarm, about 100 km-long and 70 km-wide, is much larger than one would expect given the size of the earthquakes involved in the sequence; and finally, the migration described above suggests that additional aseismic processes drove seismicity to spread over a wider area during over three weeks.

A key question remains on the depth of the seismicity, and the main earthquakes analyzed here. The regional network was limited in 2006; therefore, the depth accuracy is poorly constrained in the studied seismic catalog. The first events of the seismic swarm have low-depth uncertainties; however, we acknowledge that our scarce database did not allow us to obtain a high-resolution picture offshore, only using the information from a few inland stations. Based on the analysis of the two largest earthquakes of the sequence using teleseismic information, we can constrain the depth location of the two largest earthquakes of the sequence. For the first event, the solution converges to ~15 km depth, while the second event shows similar Normalized RMS misfits for a wider depth range, a problem likely induced by seismic ambient noise (Morales-Yáñez et al., 2020) due to the first event. Nonetheless, a shallower solution may be reliable considering also the uncertainties in the centroid depth (Fig. 6). Additionally, for all the possible estimations in-depth, both reverse focal mechanisms indicate a low-angle rupture likely associated with the fault plane. Based on our results, we suggest that the 2006 seismic swarm aforementioned occurred at the megathrust interface. However, we cannot discard the possibility of shallow seismicity occurring in the overriding plate.

4.2. Slow & fast slip during the Copiapó swarm

Earthquake swarms along the Chilean subduction zone have occurred in a diversity of modes through seismic sequences. These seismic swarms have been part of slow and fast behaviors at the plate interface, such as during the Mw 8.1 2014 Iquique and the Mw 6.9 2017 Valparaíso (e.g., Kato et al., 2016; Ruiz et al., 2014, 2017; Caballero et al., 2021). Conversely, other seismic swarms have been identified without a subsequent major event, such as the recurrent Navidad swarm in Central-South Chile (Valenzuela-Malebrán et al., 2021) or some persistent seismic swarms occurring in the Coquimbo region, North-Central Chile (Poli et al., 2017; Vigny et al., 2009) that exhibit moderate-to-low magnitude earthquakes.

The single GPS station COPO was analyzed to address if any transient signal took place during the period of the 2006 Copiapó swarm (Fig. 4). We identified a slightly westward/trenchward transient from April 19 to April 28. Precisely, this small trend change started the same day we identified the beginning of the seismic swarm while we observed a burst of seismicity occurring on April 19. Moreover, during this period, we observe higher waveform similarities between pairs of earthquakes, including doublets with a high correlation coefficient as a potential repeater event (Fig. 5 and Fig. S7). We consider that this

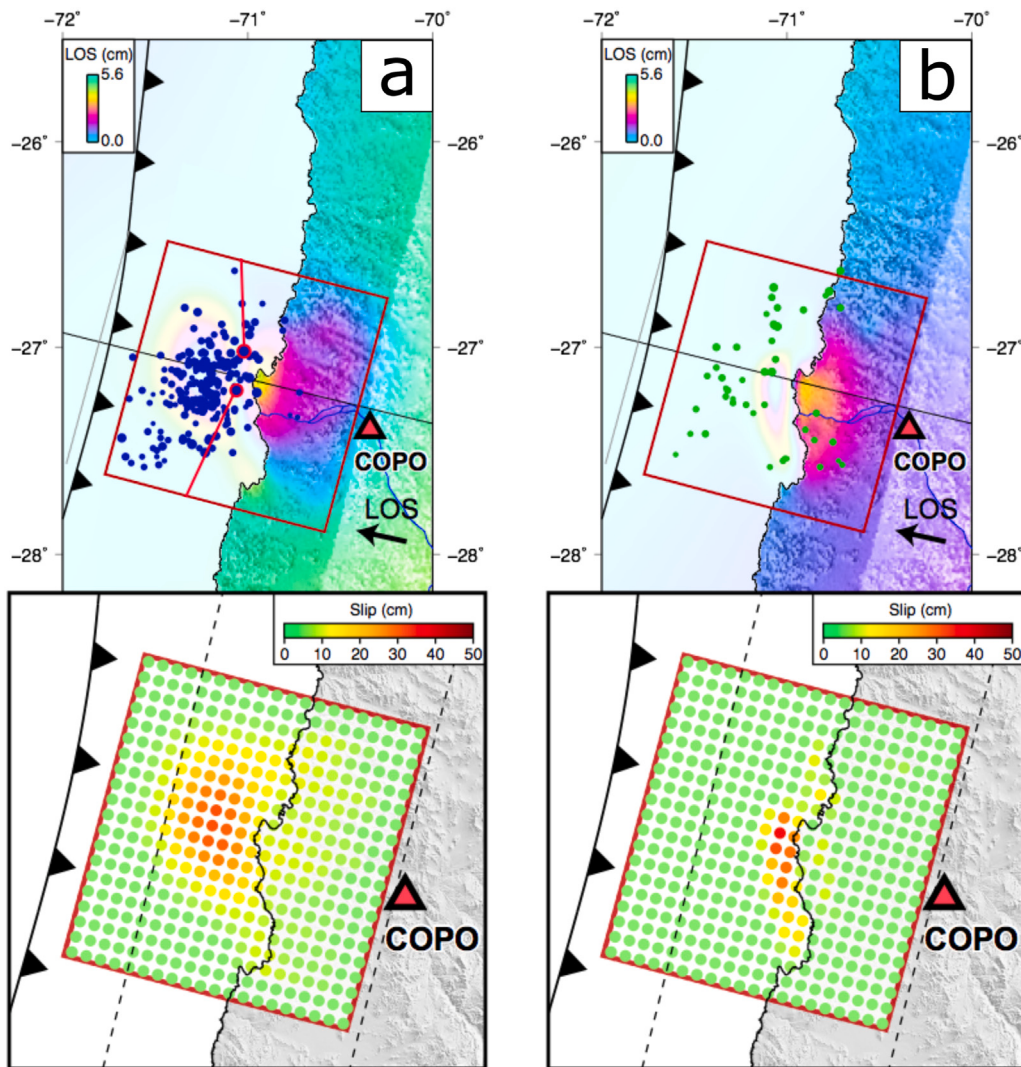


Fig. 7. Surface deformation due to the 2006 Copiapó swarm determined by InSAR and the GPS station COPPO. (a) Model of the “coseismic deformation” of the Copiapó swarm. The colors indicate the line-of-sight (LOS) component of the surface ground displacement derived from InSAR. The blue circles represent the seismic activity identified during the “coseismic” period between 2005-09-26 and 2006-07-03. The bottom panel shows the slip distribution model along the discretized surface fault. (b) Model of the “postseismic deformation” of the Copiapó swarm projected in LOS. The green circles represent the seismic activity identified as the aftershock during the “postseismic” period between 2006-07-03 and 2009-08-31. The bottom panel shows the postseismic slip model inverted along the discretized surface fault.

intensive doublet activity and the seismic swarm evolution in this first stage took place while an SSE had driven slip on the plate interface. The relative depth of the seismicity, which according to the epicentral location, could reach 15–20 km depth, suggests that this potential SSE took place at a shallow segment of the megathrust. The possible short-term SSE is not comparable to the Mexican (e.g. Radiguet et al., 2012), Cascadia (e.g. Bletry and Nocquet, 2020), or New Zealand (e.g. Wallace et al., 2012) transient signals that could reach a few centimeters of displacement due to the scarce GPS instrumentation at this time. Based on our findings, we propose that a M~6 SSE is feasible offshore along the shallowest segment of the plate interface. Around La Plata Island, Ecuador, Vallée et al. (2013) documented shallow SSE together with seismic swarms likely driven by stress fluctuations related to aseismic slip and supported by consistent families of repetitive earthquakes. Observations such as in Ecuador may indicate that seismic swarm activity and slow processes have a key role in stress release along subduction zones, and possibly these processes occur synchronously.

To further analyze the influence of the proposed SSE, we perform the inversion of the coseismic deformation of the 2006 seismic swarm from both GPS and InSAR observations (Fig. 7). We assume that the slip takes place on the subduction interface, and we carried out an

exploration of parameters on the area of the dislocation. Our results are shown in Fig. 7a and Fig. S15. The parameters that best fit the data are a slip distribution of dimensions of about 26×35 km and a maximum slip of 40 cm, located in an area that agrees with our focal mechanism solutions. This coseismic slip distribution considers a whole period that we so-called “coseismic”, but includes mainly the seismic swarm and the two largest earthquakes magnitude $M_w \sim 6.5$ – 6.6 . We also estimated the geodetic moment from our inversion, equivalent to an $M_w 6.85$, compared to the cumulative seismic moment released in the same period, equal to an $M_w 6.77$. Following these results, during the coseismic period, we observed both seismic and aseismic slips but no strong differences between them in terms of total moment released. Previously, Holtkamp et al. (2011) also performed the inversion of the coseismic deformation with only three interferograms and indicated that the model that best explains their data does not require a significant aseismic motion. However, their results show a strong residual inland around the Copiapó city that could be controlled for an important postseismic component included as a dataset of their inversion. This example motivates us to separate the postseismic contribution from the coseismic component by carefully studying the temporal inversion from a set of 55 interferograms. Our results are shown in Fig. 7b

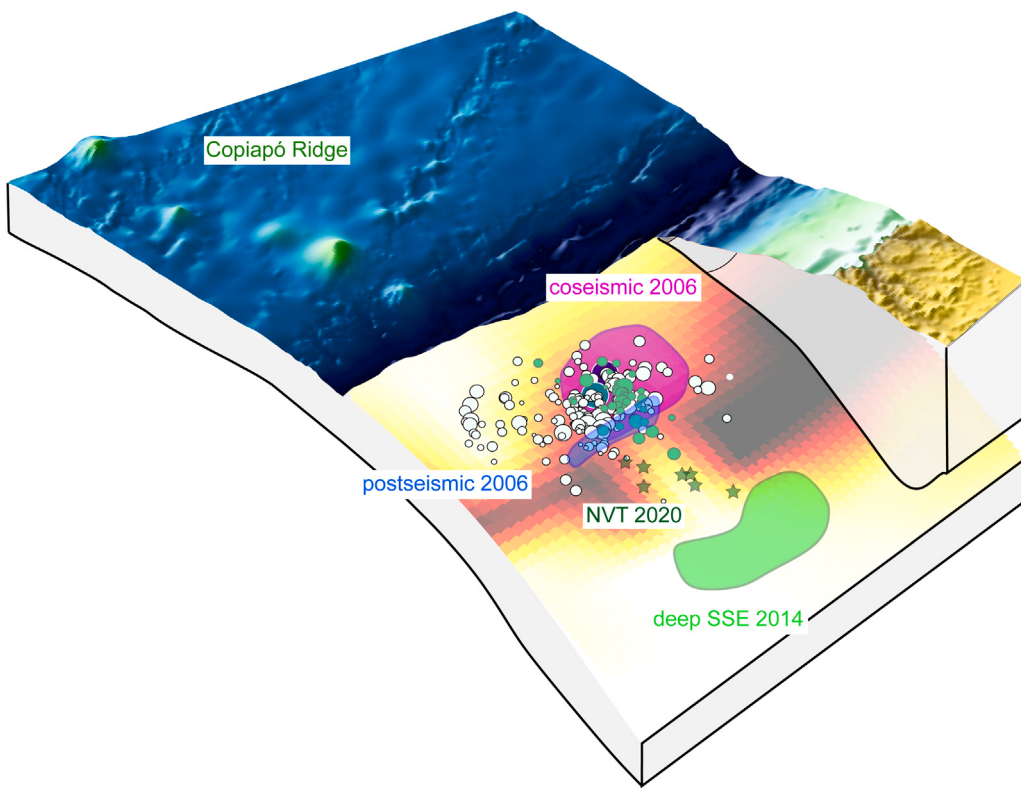


Fig. 8. Schematic summary of the diversity slips behaviors observed in Copiapó. Circles represented the seismicity during April and May 2006; the green circles correspond to the seismic swarm between April 19 to April 29, while the white circles correspond to the spreading of the seismicity after the two largest earthquakes occurring on April 30 at 19:17 (bright cyan circle) and 21:40 (purple circle). The coseismic and postseismic deformation inferred from geodetic data is placed in the violet and blue areas, respectively. The star shows the location of Non-volcanic tremors (NVT) identified in 2020 (Pastén-Araya et al., 2022) and the green area corresponds to the 2014 deep SSE (Klein et al., 2018a). The red color map along the interface shows the coupling model from Klein et al. (2018b).

and Fig. S16. Our best solution shows a dislocation taking place deeper and slightly further south than the coseismic rupture, with an average slip of about 26.5 cm. The estimated geodetic moment is equivalent to an Mw 6.6, a value several times greater than the cumulative seismic moment from this period equivalent to an Mw 5.4. These results lead us to interpret the postseismic slip occurring along the plate interface with a significant aseismic component of about 98%, which had not been highlighted before.

An interesting interplay between seismic and aseismic deformation during swarm episodes has been proposed for some segments of the South America subduction. For instance, in North-Central Chile, Klein et al. (2021) analyzed the estimated moment released by the 2020 Atacama seismic sequence, which was 60% due to earthquakes and 40% due to aseismic slip in an area of about $100 \times 100 \text{ km}^2$. Also, in Chile, during the nucleation phase of the Mw 6.9 Valparaíso earthquake sequence, Ruiz et al. (2017) proposed about 80% of aseismic slip released; conversely, Caballero et al. (2021) estimated about $51\% \pm 11\%$ of aseismic slip on the megathrust. Moreover, in northern Peru, a shallow seismic sequence that occurred in 2009 was accompanied by an SSE that lasted seven months (Villegas-Lanza et al., 2016). Given the moment released, the authors suggested that a ~70%–85% aseismic process occurred in an area of about $80 \times 80 \text{ km}^2$. In northern Ecuador, the 2013–2014 seismic swarm was jointly detected by an SSE, with the evolution of aseismic slip representing 99% of the total moment released (Vaca et al., 2018). Finally, Segovia et al. (2018) also found on La Plata Island, Ecuador, that the 2013 seismic swarm was synchronous with an SSE that released about 80% of the total moment estimated from geodetic motion. For the 2006 Copiapó swarm, we roughly estimate a ratio of the overall seismic and aseismic moment released of about 43% and 57%, respectively, which occurred in a large area of $100 \times 70 \text{ km}^2$. These relatively moderate M6–7 magnitude

sequences occurred in large areas considering the maximum magnitude earthquake of their whole sequences. In summary, although the seismic and aseismic ratio differences for these seismic swarm episodes in the South America subduction zone, similar mechanisms, such as slow slip deformation, seem to appear in most of them, suggesting a common driver of microseismicity in large extensions in which seismic swarms occur.

We synthesized our insights in Fig. 8, which include the seismic swarm, the two largest earthquakes, and the seismicity after these two major events; we also include the coseismic and postseismic deformation associated with the 2006 Copiapó swarm, as well as other aseismic signatures discovered in the area such as non-volcanic tremors (NVT) and the possible 2005 deep SSE (Pastén-Araya et al., 2022; Klein et al., 2018a). Considering the Lay et al. (2012) subduction earthquake classification, here we followed the most specific along-dip segmentation for this region proposed by Pastén-Araya et al. (2022). We observed that the recurrent deep SSE in 2005, 2009, and 2014 took place in a deeper segment of the megathrust in zone C, and the NVT activity seems to occur in zone B referred as a transitional segment that may impede the propagation of major ruptures; whereas the synchronous seismic swarm and slow slip event, including doublets events, and the spreading of the seismicity, occurred at shallow depths in zone A, the same area where similar events and potential repeater earthquakes were previously identified (Pastén-Araya et al., 2022). These aseismic signatures proposed in our work add another intriguing component to the diversity of slip behaviors previously reported in the Atacama region.

4.3. The influence of the Copiapó ridge

The presence of remarkable high-bathymetric features in the oceanic lithosphere as the Copiapó Ridge and its seamounts subducting may

play a role in the subduction processes inducing frictional segmentation along the plate interface and their surroundings (Wang and Bilek, 2011, 2014). The effects include coupling coefficient differences, a wide diversity of slip behaviors, and seismic/aseismic signatures along the plate interface, resulting in a decrease of normal stress potentially driven by fluid pressure (Poli et al., 2017). Therefore, the complexities and heterogeneities at these depths favor aseismic creep, seismic swarm, and repeater activity (Wang and Bilek, 2011; Valenzuela-Malebrán et al., 2021; Singh et al., 2011). In Copiapó, Chile, Pastén-Araya et al. (2022) inferred an along-dip heterogeneous plate interface, identifying clusters of similar events at shallow depths in the interface (between 18 to 29 km depth) occurring in a zone with a high V_p/V_s ratio and moderate V_s and V_p values, and with a low coupling value (Klein et al., 2018b; Métois et al., 2016), separating two areas of high coupling northern and southern the path of the seamounts tracking. Moreover, the 2006 Copiapó swarm occurred at the edge of a low coupling zone, which favors our hypothesis of an SSE occurring just below this shallowest segment of the plate interface where also NVT activity has been identified. These physical conditions suggest fluid content in the system that may drive or promote transient aseismic slip at that portion of the megathrust.

More recently, in Central Chile, the 2017 Valparaíso Mw 6.9 earthquake nucleated in the vicinity of a subducted seamount of the Juan Fernández Ridge (Ruiz et al., 2018). In this case, the clustered seismicity presented a migration pattern from the north to the southeast, potentially associated with an aseismic slip transient (Ruiz et al., 2017; Caballero et al., 2021). The similar nature and migration history between the Copiapó Ridge and the Juan Fernández Ridge (Bello-González et al., 2018), suggest a similar influence on the slip behaviors due to the seamounts subducted for each Ridge. In both cases, the high topographic complexities, seismicity migration, and potential aseismic process reflect an asperity-like behavior that may promote clustered low-to-moderate seismicity but also changes in the deformation process along the plate interface.

Subducted oceanic features such as oceanic ridges also indicate potential fractures of the upper plate around the subducting seamounts within the forearc regions (Wang and Bilek, 2011; Morell, 2016). For instance, in the Ecuadorian subduction zone, Collot et al. (2017) studied how the oceanic relief subducting is deforming seismic and aseismically the forearc in an area of recurrent SSE located in a partly locked region. They described that seismicity could rupture at the plate interface, and other events could reactivate near faults, while an SSE induces a stress increment and promotes complex and multiple ruptures in the seamount's surroundings. If that is the case of the 2006 Copiapó swarm, we think that the persistent and localized seismic swarm during the first period may occur at shallow depths, possibly influenced by a seamount undergoing subduction as suggested by Comte et al. (2002). The spatial location of this seamount along the interface could explain the seafloor morphology observed in the bathymetry as a response to the seamount subducting in the area (Métois et al., 2014; Comte et al., 2006). Therefore, following other authors, we consider that the tracking of the Copiapó Ridge and the spatial distribution of their seamounts may influence and trigger the diversity of seismic and aseismic signatures observed, including the 2006 seismic swarm.

5. Conclusion

We have studied the fast and slow processes related to the 2006 Copiapó swarm performing seismological and geodetic constraints. The seismic swarm occurred at a shallow area of the plate interface that spatially correlates with an inferred subducted seamount of the Copiapó Ridge at this latitude. We show a spatiotemporal evolution of the seismicity, starting with clustered earthquakes on April 19 that migrate at velocities around 2 to 10 km/day until April 28, the same period when we find high cross-correlation coefficients among pairs of events, doublets earthquakes, and a slight westward transient in

the GPS station COPO. We further study the two largest earthquakes Mw~6.5–6.6 that occur only 2.4 h apart from each other. The focal mechanism, centroid depth, and time shift solutions allow us to propose similarities between them, confirming a low-angle mechanism, shallow depths constrained to the plate interface, and similar rupture patterns. We characterized the coseismic and postseismic deformation related to the seismic swarm by using InSAR images, from which we conclude a significant contribution of aseismic slip during the postseismic period, while during the coseismic period, we identify a more negligible contribution. We proposed that the 2006 Copiapó swarm and their migration patterns observed during the initial period were driven by a potential slow slip event likely influenced by the presence of the Copiapó Ridge, which decoupled the plate interface and promoted aseismic signatures such as NVT, repetitive earthquakes, and shallow and deep SSE, previously studied. Finally, despite the data limitations during this period, we further attempt to study the large seismic swarm hosted in an area where large earthquakes such as the 1922 Atacama event have occurred and where it has been a challenge to assess for seismic hazard evaluation, including the potential influence of the slip behavior diversity.

CRediT authorship contribution statement

Javier Ojeda: Writing – review & editing, Writing – original draft, Visualization, Software, Methodology, Investigation, Formal analysis, Conceptualization. **Catalina Morales-Yáñez:** Writing – review & editing, Writing – original draft, Software, Methodology, Data curation. **Gabriel Ducret:** Writing – review & editing, Methodology, Data curation. **Sergio Ruiz:** Writing – review & editing, Writing – original draft, Supervision, Conceptualization. **Raphael Grandin:** Writing – review & editing, Writing – original draft, Methodology, Data curation. **Marie-Pierre Doin:** Writing – review & editing, Methodology, Data curation. **Christophe Vigny:** Writing – review & editing. **Jean-Mathieu Nocquet:** Writing – review & editing, Formal analysis, Investigation.

Declaration of competing interest

The authors declare that they have no known competing financial interests or personal relationships that could have appeared to influence the work reported in this paper.

Data availability

Data will be made available on request.

Acknowledgments

We wish to thank the network and station operators for their commitment to collect high-quality seismic data. The seismic catalog was provided by the Centro Sismológico Nacional (CSN, Chile; <http://www.sismologia.cl/>, last accessed 2022 May 31). Seismological data and metadata were accessed through the IRIS web service; we used a combination of channels from GEONET (GE), GEOSCOPE (G), ASL/USGS (IU,GT), IRIS/IDA (II), Pacific21 (PS) and BDSN (BK). The processing, mapping, and visualization of this article were benefited from various python packages, including matplotlib (Hunter, 2007), obspy (Krischer et al., 2015), and pygmt (Uieda et al., 2021, using 3 arc second global relief from SRTM3S). JO acknowledges support from the Agencia Nacional de Investigación y Desarrollo scholarship ANID-PFCHA/Doctorado Nacional/2020-21200903. CMY acknowledges funding from ANID/FONDECYT 3220307 and thanks the support of the Anillo precursor project ANID PIA Anillo ACT192169. SR thanks ANID/FONDECYT project no. 1200779. We thank the Agence Nationale de la Recherche (ANR), S5 project: "Synchronous Slow Slip & Seismic Swarm", grant ANR-19-CE31-0003-01. Finally, the authors thank two anonymous reviewers and the Editor, E. Contreras-Reyes, for their constructive comments and suggestions that helped us to improve the original manuscript.

Appendix A. Supplementary data

Supplementary material related to this article can be found online at <https://doi.org/10.1016/j.jsames.2023.104198>.

References

- Abad, M., Izquierdo, T., Cáceres, M., Bernárdez, E., Rodríguez-Vidal, J., 2020. Coastal boulder deposit as evidence of an ocean-wide prehistoric tsunami originated on the Atacama Desert coast (Northern Chile). *Sedimentology* 67 (3), 1505–1528. <http://dx.doi.org/10.1111/sed.12570>.
- Álvarez, O., Giménez, M., Folguera, A., Spagnotto, S., Bustos, E., Baez, W., Braatenberg, C., 2015. New evidence about the subduction of the Copiapó ridge beneath South America, and its connection with the Chilean-Pampas flat slab, tracked by satellite GOCE and EGM2008 models. *J. Geodyn.* 91, 65–88. <http://dx.doi.org/10.1016/j.jog.2015.08.002>.
- Barrientos, S., 2018. The seismic network of Chile. *Seismol. Res. Lett.* 89 (2A), 467–474. <http://dx.doi.org/10.1785/0220160195>.
- Beck, S., Barrientos, S., Kausel, E., Reyes, M., 1998. Source characteristics of historic earthquakes along the Central Chile subduction Askew et Alzone. *J. South Am. Earth Sci.* 11 (2), 115–129. [http://dx.doi.org/10.1016/S0895-9811\(98\)00005-4](http://dx.doi.org/10.1016/S0895-9811(98)00005-4).
- Bello-González, J.P., Contreras-Reyes, E., Arriagada, C., 2018. Predicted path for hotspot tracks off South America since Paleocene times: Tectonic implications of ridge-trench collision along the Andean margin. *Gondwana Res.* 64, 216–234. <http://dx.doi.org/10.1016/j.gr.2018.07.008>.
- Bleiter, Q., Nocquet, J.-M., 2020. Slip bursts during coalescence of slow slip events in Cascadia. *Nature Commun.* 11 (1), 1–6. <http://dx.doi.org/10.1038/s41467-020-15494-4>.
- Caballero, E., Chouvet, A., Duputel, Z., Jara, J., Twardzik, C., Jolivet, R., 2021. Seismic and aseismic fault slip during the initiation phase of the 2017 MW=6.9 Valparaíso earthquake. *Geophys. Res. Lett.* 48 (6), e2020GL091916. <http://dx.doi.org/10.1029/2020GL091916>.
- Carvajal, M., Cisternas, M., Gubler, A., Catalán, P., Winckler, P., Wesson, R.L., 2017. Reexamination of the magnitudes for the 1906 and 1922 Chilean earthquakes using Japanese tsunami amplitudes: Implications for source depth constraints. *J. Geophys. Res. Solid Earth* 122 (1), 4–17. <http://dx.doi.org/10.1002/2016JB013269>.
- Collot, J.Y., Sanclemente, E., Nocquet, J.-M., Leprétre, A., Ribodetti, A., Jarrín, P., Chlieh, M., Graindorge, D., Charvis, P., 2017. Subducted oceanic relief locks the shallow megathrust in central Ecuador. *J. Geophys. Res. Solid Earth* 122 (5), 3286–3305. <http://dx.doi.org/10.1002/2016JB013849>.
- Comte, D., Haessler, H., Dobrath, L., Pardo, M., Monfre, T., Lavenu, A., Pontoise, B., Hello, Y., 2002. Seismicity and stress distribution in the Copiapo, Northern Chile subduction zone using combined on-and off-shore seismic observations. *Phys. Earth Planet. Inter.* 132 (1–3), 197–217. [http://dx.doi.org/10.1016/S0031-9201\(02\)00052-3](http://dx.doi.org/10.1016/S0031-9201(02)00052-3).
- Comte, D., Tassara, A., Farias, M., Boroschek, R., 2006. 2006 Copiapo Chile seismic swarm analysis: mapping the interplate contact. In: AGU Fall Meeting Abstracts, Vol. 2006. pp. S53B-1327.
- Contreras-Reyes, E., Carrizo, D., 2011. Control of high oceanic features and subduction channel on earthquake ruptures along the Chile–Peru subduction zone. *Phys. Earth Planet. Inter.* 186 (1–2), 49–58. <http://dx.doi.org/10.1016/j.pepi.2011.03.002>.
- Das, S., Watts, A., 2009. Effect of subducting seafloor topography on the rupture characteristics of great subduction zone earthquakes. In: Subduction Zone Geodynamics. Springer, pp. 103–118. http://dx.doi.org/10.1007/978-3-540-87974-9_6.
- Ducret, G., Doin, M.P., Grandin, R., Lasserre, C., Guillou, S., 2013. DEM corrections before unwrapping in a small baseline strategy for InSAR time series analysis. *IEEE Geosci. Remote Sens. Lett.* 11 (3), 696–700. <http://dx.doi.org/10.1109/LGRS.2013.2276040>.
- Duputel, Z., Rivera, L., 2019. The 2007 caldera collapse of Piton de la Fournaise volcano: Source process from very-long-period seismic signals. *Earth Planet. Sci. Lett.* 527, 115786. <http://dx.doi.org/10.1016/j.epsl.2019.115786>.
- Dziewonski, A.M., Chou, T.A., Woodhouse, J.H., 1981. Determination of earthquake source parameters from waveform data for studies of global and regional seismicity. *J. Geophys. Res. Solid Earth* 86 (B4), 2825–2852. <http://dx.doi.org/10.1029/JB086IB04p02825>.
- Ekström, G., Nettles, M., Dziewoński, A., 2012. The global CMT project 2004–2010: Centroid-moment tensors for 13,017 earthquakes. *Phys. Earth Planet. Inter.* 200, 1–9. <http://dx.doi.org/10.1016/j.pepi.2012.04.002>.
- Grandin, R., Doin, M.P., Bollinger, L., Pinel-Puisségur, B., Ducret, G., Jolivet, R., Sapkota, S.N., 2012. Long-term growth of the himalaya inferred from interseismic InSAR measurement. *Geology* 40 (12), 1059–1062. <http://dx.doi.org/10.1130/G33154.1>.
- Hayes, G.P., Moore, G.L., Portner, D.E., Hearne, M., Flamme, H., Furtney, M., Smoczyk, G.M., 2018. Slab2, a comprehensive subduction zone geometry model. *Science* 362 (6410), 58–61. <http://dx.doi.org/10.1126/science.aat4723>.
- Holtkamp, S.G., Pritchard, M., Lohman, R., 2011. Earthquake swarms in South America. *Geophys. J. Int.* 187 (1), 128–146. <http://dx.doi.org/10.1111/j.1365-246X.2011.05137.x>.
- Hoskins, M.C., Meltzer, A., Font, Y., Agurto-Detzel, H., Vaca, S., Rolandone, F., Nocquet, J.-M., Soto-Cordero, L., Stachnik, J.C., Beck, S., et al., 2021. Triggered crustal earthquake swarm across subduction segment boundary after the 2016 Pedernales, Ecuador megathrust earthquake. *Earth Planet. Sci. Lett.* 553, 116620. <http://dx.doi.org/10.1016/j.epsl.2020.116620>.
- Hunter, J.D., 2007. Matplotlib: A 2D graphics environment. *Comput. Sci. Eng.* 9 (3), 90–95. <http://dx.doi.org/10.1109/MCSE.2007.55>.
- Jolivet, R., Grandin, R., Lasserre, C., Doin, M.P., Peltzer, G., 2011. Systematic InSAR tropospheric phase delay corrections from global meteorological reanalysis data. *Geophys. Res. Lett.* 38 (17), <http://dx.doi.org/10.1029/2011GL048757>.
- Kanamori, H., Rivera, L., Ye, L., Lay, T., Murotani, S., Tsumura, K., 2019. New constraints on the 1922 Atacama, Chile, earthquake from historical seismograms. *Geophys. J. Int.* 219 (1), 645–661. <http://dx.doi.org/10.1093/gji/ggz302>.
- Kato, A., Fukuda, J., Kumazawa, T., Nakagawa, S., 2016. Accelerated nucleation of the 2014 Iquique, Chile Mw 8.2 earthquake. *Sci. Rep.* 6 (1), 1–9. <http://dx.doi.org/10.1038/srep24792>.
- Klein, E., Duputel, Z., Zigone, D., Vigny, C., Boy, J.P., Doubre, C., Meneses, G., 2018a. Deep transient slow slip detected by survey GPS in the region of Atacama, Chile. *Geophys. Res. Lett.* 45 (22), 12–263. <http://dx.doi.org/10.1029/2018GL080613>.
- Klein, E., Metois, M., Meneses, G., Vigny, C., Delorme, A., 2018b. Bridging the gap between North and Central Chile: insight from new GPS data on coupling complexities and the Andean sliver motion. *Geophys. J. Int.* 213 (3), 1924–1933. <http://dx.doi.org/10.1093/gji/ggy094>.
- Klein, E., Potin, B., Pasten-Araya, F., Tissandier, R., Azua, K., Duputel, Z., Herrera, C., Rivera, L., Nocquet, J.-M., Baez, J.C., et al., 2021. Interplay of seismic and a-seismic deformation during the 2020 sequence of Atacama, Chile. *Earth Planet. Sci. Lett.* 570, 117081. <http://dx.doi.org/10.1016/j.epsl.2021.117081>.
- Klein, E., Vigny, C., Duputel, Z., Zigone, D., Rivera, L., Ruiz, S., Potin, B., 2023. Return of the Atacama deep Slow Slip Event: The 5-year recurrence confirmed by continuous GPS. *Phys. Earth Planet. Inter.* 334, 106970. <http://dx.doi.org/10.1016/j.pepi.2022.106970>.
- Klein, E., Vigny, C., Nocquet, J.-M., Boulze, H., 2022. A 20 year-long GNSS solution across South-America with focus in Chile. *BSGF - Earth Sci. Bull.* 193 (1), <http://dx.doi.org/10.1051/bsgf/2022005>.
- Krischer, L., Megies, T., Barsch, R., Beyreuther, M., Lecocq, T., Caudron, C., Wassermann, J., 2015. ObsPy: A bridge for seismology into the scientific Python ecosystem. *Comput. Sci. Discov.* 8 (1), 014003. <http://dx.doi.org/10.1088/1749-4699/8/1/014003>.
- Lay, T., Kanamori, H., Ammon, C.J., Koper, K.D., Hutko, A.R., Ye, L., Yue, H., Rushing, T.M., 2012. Depth-varying rupture properties of subduction zone megathrust faults. *J. Geophys. Res. Solid Earth* 117 (B4), <http://dx.doi.org/10.1029/2011JB009133>.
- Maksmowicz, A., 2015. The geometry of the Chilean continental wedge: Tectonic segmentation of subduction processes off Chile. *Tectonophysics* 659, 183–196. <http://dx.doi.org/10.1016/j.tecto.2015.08.007>.
- Manea, V.C., Leeman, W.P., Gerya, T., Manea, M., Zhu, G., 2014. Subduction of fracture zones controls mantle melting and geochemical signature above slabs. *Nature Commun.* 5 (1), 1–10. <http://dx.doi.org/10.1038/ncomms6095>.
- Metois, M., Vigny, C., Socquet, A., 2016. Interseismic coupling, megathrust earthquakes and seismic swarms along the Chilean subduction zone (38–18 s). *Pure Appl. Geophys.* 173 (5), 1431–1449. <http://dx.doi.org/10.1007/s00024-016-1280-5>.
- Metois, M., Vigny, C., Socquet, A., Delorme, A., Morvan, S., Ortega, I., Valderas-Bermejo, C.-M., 2014. GPS-derived interseismic coupling on the subduction and seismic hazards in the Atacama region, Chile. *Geophys. J. Int.* 196 (2), 644–655. <http://dx.doi.org/10.1093/gji/ggt418>.
- Morales-Yáñez, C., Duputel, Z., Rivera, L., 2020. Impact of 3-D Earth structure on W-phase CMT parameters. *Geophys. J. Int.* 223 (2), 1432–1445. <http://dx.doi.org/10.1093/gji/ggaa377>.
- Morell, K.D., 2016. Seamount, ridge, and transform subduction in Southern Central America. *Tectonics* 35 (2), 357–385. <http://dx.doi.org/10.1002/2015TC003950>.
- Nishikawa, T., Ide, S., 2015. Background seismicity rate at subduction zones linked to slab-bending-related hydration. *Geophys. Res. Lett.* 42 (17), 7081–7089. <http://dx.doi.org/10.1002/2015GL064578>.
- Nishikawa, T., Ide, S., 2017. Detection of earthquake swarms at subduction zones globally: Insights into tectonic controls on swarm activity. *J. Geophys. Res. Solid Earth* 122 (7), 5325–5343. <http://dx.doi.org/10.1002/2017JB014188>.
- Okada, Y., 1985. Surface deformation due to shear and tensile faults in a half-space. *Bull. Seismol. Soc. Am.* 75 (4), 1135–1154. <http://dx.doi.org/10.1785/BSSA0750041135>.
- Pastén-Araya, F., Potin, B., Azua, K., Saez, M., Aden-Antoniów, F., Ruiz, S., Cabrera, L., Ampuero, J.P., Nocquet, J.-M., Rivera, L., et al., 2022. Along-dip segmentation of the slip behavior and rheology of the Copiapó ridge subducted in North-Central Chile. *Geophys. Res. Lett.* 49 (4), e2021GL095471. <http://dx.doi.org/10.1029/2021GL095471>.
- Peacock, S.A., 1990. Fluid processes in subduction zones. *Science* 248 (4953), 329–337. <http://dx.doi.org/10.1126/science.248.4953.329>.
- Poli, P., Maksmowicz, A., Ruiz, S., 2017. The Mw 8.3 Illapel earthquake (Chile): Pre-seismic and postseismic activity associated with hydrated slab structures. *Geology* 45 (3), 247–250. <http://dx.doi.org/10.1130/G38522.1>.

- Radiguet, M., Cotton, F., Vergnolle, M., Campillo, M., Walpersdorf, A., Cotte, N., Kostoglodov, V., 2012. Slow slip events and strain accumulation in the Guerrero gap, Mexico. *J. Geophys. Res. Solid Earth* 117 (B4), <http://dx.doi.org/10.1029/2011JB008801>.
- Ruiz, S., Aden-Antoniow, F., Baez, J.C., Otarola, C., Potin, B., Del Campo, F., Poli, P., Flores, C., Satriano, C., Leyton, F., et al., 2017. Nucleation phase and dynamic inversion of the Mw 6.9 Valparaíso 2017 earthquake in Central Chile. *Geophys. Res. Lett.* 44 (20), 10–290. <http://dx.doi.org/10.1002/2017GL075675>.
- Ruiz, J.A., Contreras-Reyes, E., Ortega-Culaciati, F., Maríquez, P., 2018. Rupture process of the April 24, 2017, Mw 6.9 Valparaíso earthquake from the joint inversion of teleseismic body waves and near-field data. *Phys. Earth Planet. Inter.* 279, 1–14. <http://dx.doi.org/10.1016/j.pepi.2018.03.007>.
- Ruiz, S., Grandin, R., Dionicio, V., Satriano, C., Fuenzalida, A., Vigny, C., Kiraly, E., Meyer, C., Baez, J.C., Riquelme, S., et al., 2013. The Constitución earthquake of 25 March 2012: a large aftershock of the Maule earthquake near the bottom of the seismogenic zone. *Earth Planet. Sci. Lett.* 377, 347–357. <http://dx.doi.org/10.1016/j.epsl.2013.07.017>.
- Ruiz, S., Madariaga, R., 2018. Historical and recent large megathrust earthquakes in Chile. *Tectonophysics* 733, 37–56. <http://dx.doi.org/10.1016/j.tecto.2018.01.015>.
- Ruiz, S., Metois, M., Fuenzalida, A., Ruiz, J., Leyton, F., Grandin, R., Vigny, C., Madariaga, R., Campos, J., 2014. Intense foreshocks and a slow slip event preceded the 2014 Iquique M w 8.1 earthquake. *Science* 345 (6201), 1165–1169. <http://dx.doi.org/10.1126/science.1256074>.
- Salazar, D., Easton, G., Goff, J., Guendón, J.L., González-Alfaro, J., Andrade, P., Villagrán, X., Fuentes, M., León, T., Abad, M., et al., 2022. Did a 3800-year-old Mw 9.5 earthquake trigger major social disruption in the Atacama Desert? *Sci. Adv.* 8 (14), eabm2996. <http://dx.doi.org/10.1126/sciadv.abm2996>.
- Segovia, M., Font, Y., Régnier, M., Charvis, P., Galve, A., Nocquet, J.-M., Jarrín, P., Hello, Y., Ruiz, M., Pazmiño, A., 2018. Seismicity distribution near a subducting seamount in the Central Ecuadorian subduction zone, space-time relation to a slow-slip event. *Tectonics* 37 (7), 2106–2123. <http://dx.doi.org/10.1029/2017TC004771>.
- Shapiro, S.A., Huenges, E., Borm, G., 1997. Estimating the crust permeability from fluid-injection-induced seismic emission at the KTB site. *Geophys. J. Int.* 131 (2), F15–F18. <http://dx.doi.org/10.1111/j.1365-246X.1997.tb01215.x>.
- Shapiro, S.A., Patzig, R., Rothert, E., Rindschwendner, J., 2003. Triggering of seismicity by pore-pressure perturbations: Permeability-related signatures of the phenomenon. In: Thermo-Hydro-Mechanical Coupling in Fractured Rock. Springer, pp. 1051–1066. http://dx.doi.org/10.1007/978-3-0348-8083-1_16.
- Shelly, D.R., Berroza, G.C., Ide, S., 2007. Complex evolution of transient slip derived from precise tremor locations in Western Shikoku, Japan. *Geochem. Geophys. Geosyst.* 8 (10), <http://dx.doi.org/10.1029/2007GC001640>.
- Singh, S.C., Hananto, N., Mukti, M., Robinson, D.P., Das, S., Chauhan, A., Carton, H., Gratacos, B., Midnet, S., Djajadihardja, Y., et al., 2011. Aseismic zone and earthquake segmentation associated with a deep subducted seamount in Sumatra. *Nat. Geosci.* 4 (5), 308–311. <http://dx.doi.org/10.1038/ngeo1119>.
- Tissandier, R., Nocquet, J.-M., Klein, E., Vigny, C., Ojeda, J., Ruiz, S., 2023. Afterslip of the Mw 8.3 2015 Illapel earthquake imaged through a time-dependent inversion of continuous and survey GNSS data. *J. Geophys. Res. Solid Earth* e2022JB024778. <http://dx.doi.org/10.1029/2022JB024778>.
- Uchida, N., 2019. Detection of repeating earthquakes and their application in characterizing slow fault slip. *Prog. Planet. Sci.* 6, <http://dx.doi.org/10.1186/s40645-019-0284-z>.
- Uchida, N., Bürgmann, R., 2019. Repeating earthquakes. *Annu. Rev. Earth Planet. Sci.* 47, 305–332. <http://dx.doi.org/10.1146/annurev-earth-053018-060119>.
- Uieda, L., Tian, D., Leong, W.J., Schlitzer, W., Toney, L., Grund, M., Jones, M., Yao, J., Materna, K., Newton, T., Anant, A., Ziebarth, M., Wessel, P., 2021. PyGMT: A Python Interface for the Generic Mapping Tools. Zenodo, <http://dx.doi.org/10.5281/zenodo.4978645>.
- Vaca, S., Vallée, M., Nocquet, J.-M., Battaglia, J., Régnier, M., 2018. Recurrent slow slip events as a barrier to the northward rupture propagation of the 2016 Pedernales earthquake (Central Ecuador). *Tectonophysics* 724, 80–92. <http://dx.doi.org/10.1016/j.tecto.2017.12.012>.
- Valenzuela-Malebrán, C., Cesca, S., Ruiz, S., Passarelli, L., Leyton, F., Hainzl, S., Potin, B., Dahm, T., 2021. Seismicity clusters in Central Chile: investigating the role of repeating earthquakes and swarms in a subduction region. *Geophys. J. Int.* 224 (3), 2028–2043. <http://dx.doi.org/10.1093/gji/ggaa562>.
- Vallée, M., Nocquet, J.-M., Battaglia, J., Font, Y., Segovia, M., Régnier, M., Mothes, P., Jarrín, P., Cisneros, D., Vaca, S., et al., 2013. Intense interface seismicity triggered by a shallow slow slip event in the Central Ecuador subduction zone. *J. Geophys. Res. Solid Earth* 118 (6), 2965–2981. <http://dx.doi.org/10.1002/jgrb.50216>.
- Vigny, C., Rudloff, A., Ruegg, J.C., Madariaga, R., Campos, J., Alvarez, M., 2009. Upper plate deformation measured by GPS in the Coquimbo Gap, Chile. *Phys. Earth Planet. Inter.* 175 (1–2), 86–95. <http://dx.doi.org/10.1016/j.pepi.2008.02.013>.
- Villegas-Lanza, J.C., Nocquet, J.-M., Rolandone, F., Vallée, M., Tavera, H., Bondoux, F., Tran, T., Martin, X., Chlieh, M., 2016. A mixed seismic–aseismic stress release episode in the Andean subduction zone. *Nat. Geosci.* 9 (2), 150–154. <http://dx.doi.org/10.1038/ngeo2620>.
- Wallace, L.M., Beavan, J., Bannister, S., Williams, C., 2012. Simultaneous long-term and short-term slow slip events at the Hikurangi subduction margin, New Zealand: Implications for processes that control slow slip event occurrence, duration, and migration. *J. Geophys. Res. Solid Earth* 117 (B11), <http://dx.doi.org/10.1029/2012JB009489>.
- Wang, K., Bilek, S.L., 2011. Do subducting seamounts generate or stop large earthquakes? *Geology* 39 (9), 819–822. <http://dx.doi.org/10.1130/G31856.1>.
- Wang, K., Bilek, S.L., 2014. Fault creep caused by subduction of rough seafloor relief. *Tectonophysics* 610, 1–24. <http://dx.doi.org/10.1016/j.tecto.2013.11.024>.